ENSO Influence on Intraday Solar Irradiance in Uruguay During the Most Affected Period (Nov-Dec)

Agustín Laguarda[1], Belén Espino[1], Alejandra De Vera[2] and Rafael Terra[2]

[1]Laboratorio de Energía Solar / Instituto de Física, Facultad de Ingeniería, Universidad de la República, Montevideo (Uruguay)

[2] Instituto de Mecánica de los Fluidos e Ingeniería Ambiental, Facultad de Ingeniería, Universidad de la República, Montevideo (Uruguay)

Abstract

This work explores how El Niño Southern Oscillation (ENSO) modulates intraday to interannual solar irradiance patterns in Southeastern South America during the November-December period, when ENSO impacts on the region, in particular on radiation, are known to peak. Based on 24 years of hourly Global Horizontal Irradiance (GHI) estimates from an accurate satellite-based model, diurnal cycles of the clearness index (kt) were analyzed and grouped using K-means clustering. Four characteristic intraday patterns were identified: overcast (OC), clear-sky (CL), clear-morning/cloudy-afternoon (CL-AM), and cloudy-morning/clear-afternoon (CL-PM). Their frequencies vary significantly with ENSO phase: CL days dominate during La Niña years, while El Niño years exhibit more OC and CL-AM days. This provides a first indication of ENSO-related modulation of intraday irradiance variability. Ongoing work will extend the analysis to other periods, particularly February-May, and address spatial variability over a broader region and underlying physical mechanisms.

Keywords: GHI, daily profiles, ENSO, intraday variability, clustering

1. Introduction

Understanding solar irradiance variability is key in solar photovoltaic (PV) system planning and operation. In regions influenced by the El Niño Southern Oscillation (ENSO) phenomenon, interannual climate variability strongly modulates cloudiness and thus surface irradiance. In southeastern South America (SESA), the ENSO impact is well established (Grimm et al., 2000), and in northern Uruguay, previous studies have documented significant ENSO-driven anomalies in solar radiation (Laguarda et al., 2020a). That study, based on daily and monthly aggregated global horizontal irradiance (GHI) data, identified November–December (ND) as the most affected period, followed by February-May, with La Niña events associated with clearer conditions and El Niño years with increased cloudiness. However, that analysis did not explore ENSO's influences on the diurnal irradiance cycle or on intraday cloud regimes, relevant factors for PV generation modeling and short-term forecasting. This study represents a first step toward understanding the influence of ENSO on the intraday behavior of solar irradiance in northern Uruguay. This region is of particular interest because it combines the highest solar potential in the country (Alonso-Suárez et al., 2014), the largest installed PV capacity, and the strongest ENSO-related climatic signal. Several indices are used to quantify the ENSO cycle, here we select the commonly used Niño 3.4 index (N3.4), which represents the average sea surface temperature anomaly over a region of the central equatorial Pacific (5°N-5°S, 170°W-120°W; Trenberth, 1997). We focus on the ND period, for which the ENSO signal is known to be most prominent in the region, as captured by N3.4 averaged over the November-December-January (NDJ) season (Laguarda, 2020a). The analysis is based on long-term GHI hourly data and aims to identify systematic changes in daily irradiance profiles and their frequency of occurrence under different ENSO phases.

2. Data

2.1 Irradiance data

The study uses surface Global Horizontal Irradiance (GHI) and the clearness index (kt), defined as the ratio between GHI and the extraterrestrial solar irradiance on a horizontal plane. This index serves as a proxy for the atmosphere's global transmittance, decreasing the influence of solar geometry and isolating atmospheric effects, mainly cloudiness but also aerosols, and water vapor.

Hourly long-term GHI series were generated using the LCIM model (Laguarda et al., 2020b), a semi-empirical solar radiation model based on GOES-East geostationary satellite imagery, specifically trained for the Pampa Húmeda region (including Uruguay) and the SESA region. The LCIM belongs to the family of *Cloud Index Models (CIM)*, which estimates all-sky irradiance (I) by modulating a clear-sky radiation model through a cloud index, derived from satellite-retrieved visible reflectance:

$$I = I_{cs} \times F(C), \qquad \text{(eq. 1)}$$

where I_{cs} represents the irradiance under clear sky conditions, in this case obtained from ESRA model (Rigollier, 2000), and *F* is a function of the cloud index, C. The cloud index is obtained by normalizing the apparent albedo of each pixel between clear and overcast sky reference values, and its relationship with the clear-sky index is calibrated locally using ground measurements (Laguarda et al., 2020b). This hybrid structure allows the model to retain a physical basis while capturing regional atmospheric characteristics.

The LCIM model uses information from the visible channel of the GOES-East series of geostationary satellites (75ºW longitude over the Equator). Since the analyzed period (2000-2023) spans multiple satellite generations (GOES-8, GOES-12, GOES-13, and the more recent GOES-16 and GOES-19), the spatial resolution and temporal frequency of the imagery have evolved over time. Earlier satellites typically provided two visible images per hour at irregular intervals, whereas current GOES-16 and 19 deliver full-disk imagery every 10 minutes for South America. To ensure temporal consistency throughout the record, the analysis was performed using hourly averages.

This model has been validated in several studies (Laguarda et al., 2020b; 2021; 2023; Sarazola et al., 2023) and provides reliable GHI estimates with low uncertainty, exhibiting average root-mean-square deviation (RMSD) values below 12% (relative to the mean of ground measurements) for hourly estimates and about 6% for daily averages (Sarazola et al., 2023). Over the study region, its performance compares favorably with other satellite-based global radiation models commonly used, such as the National Renewable Energy Laboratory's (NREL) physical model PSM (Sengupta et al., 2018), which also relies on GOES imagery, and the Copernicus Atmospheric Monitoring Service (CAMS) Heliosat-4 (Qu et al., 2014), based on Meteosat satellites.

The model was used to estimate hourly GHI over 14 northern Uruguay sites for the 24-year period (2000-2023). Results are presented here for one representative site, corresponding to latitude = -30.419 and longitude = -57.461.

2.2 ENSO signal

Years were classified into El Niño, La Niña, or Neutral phases based on the N3.4 index (Trenberth, 1997), using the November-December-January (NDJ) averaged values and adopting a ±0.5 °C threshold to define ENSO conditions (Pisciottano, 1994; Laguarda, 2020a).

The N3.4 index represents the sea surface temperature anomaly in the central equatorial Pacific (5° N-5° S, 170° W-120° W), where a strong ocean-atmosphere coupling occurs (Trenberth, 1997). Positive N3.4 anomalies correspond to El Niño events, characterized by anomalous warming of the central equatorial Pacific and enhanced atmospheric convection over that region (Trenberth, 1997; McPhaden et al., 2006), whereas negative anomalies indicate La Niña conditions.

These large-scale circulation changes modulate precipitation and cloudiness patterns over the SESA region, particularly during the austral spring-summer period (Grimm et al., 2000; Pisciottano et al., 1994; De Vera et. al, 2018). In Uruguay, this affects solar irradiance mainly through changes in cloud cover: El Niño

(positive anomalies) is generally associated with increased cloudiness and reduced surface radiation, whereas La Niña events tend to produce clearer conditions and enhanced irradiance. The NDJ averaging window was selected because it captures the ENSO peak phase and its maximum radiative impact over the region, with November–December being the most affected months (Laguarda et al., 2020a).

Figure 1 shows the evolution of the N3.4-NDJ index for 2000-2024, used to classify each year as Niño, Niña or neutral. Among the 25 years, 8 were classified as Niño, 11 as Niña and 6 as neutral. This classification was used to stratify both daily and intraday irradiance analyses described in the next section.

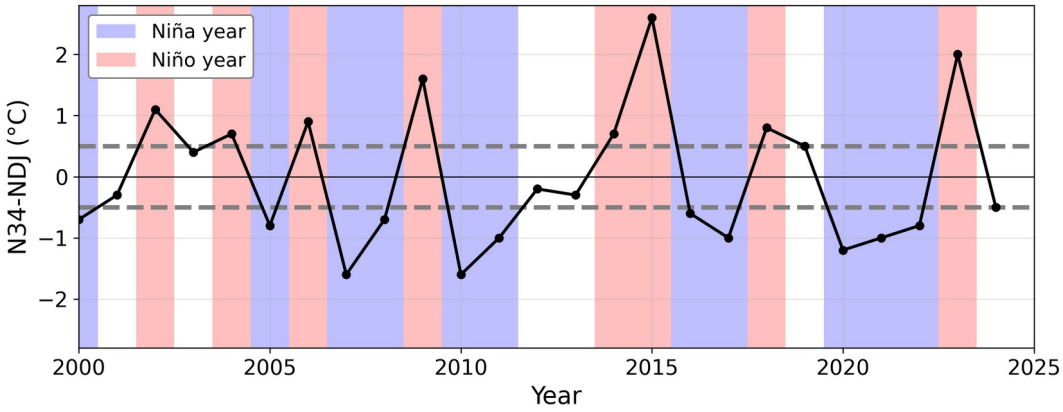

Figure 1. Evolution of the N3.4 index for the November-December-January (NDJ) season during 2000-2025. Shaded colors indicate the ENSO phase for each year: El Niño (red), La Niña (blue), and neutral (white).

3. Methodology

To assess the influence of ENSO on solar irradiance variability, two complementary analyses were performed. The first focuses on changes in the daily aggregated irradiance under different ENSO phases, while the second examines the intraday variability by clustering hourly profiles and analyzing their frequency of occurrence.

3.1 Daily scale analysis

For each day, the total daily GHI and the corresponding daily clearness index, kt, were obtained. The distribution of these daily values was analyzed for different ENSO phases. To identify whether the ENSO phases are associated with systematic shifts in the distribution of daily irradiance, the empirical cumulative distribution functions (CDFs) of the daily series were constructed separately for each subset and compared using the Kolmogorov-Smirnov (K-S) test (Massey, 1951; Wilks, 2011).

This nonparametric test assumes, as its null hypothesis, that both samples come from the same probability distribution. This hypothesis is evaluated by observing the absolute difference between the CDFs:

$$DIF(x) = |CDF_1(x) - CDF_2(x)| , \quad \text{(eq. 2)}$$

where $CDF_1(x)$ and $CDF_2(x)$ represent the empirical CDFs of two samples (e.g., El Niño vs. all years). For a given significance level (p-value), a threshold D is defined. If $DIF(x)>D$ for any x, the null hypothesis is rejected (Massey, 1951), indicating a statistically significant ENSO-related change in the daily irradiation distribution.

3.2 Intraday scale analysis

As a second approach, the intraday irradiance variability was investigated through hourly series clustering

analysis. Specifically, a K-means algorithm was applied to the clearness index diurnal cycles (Wilks, 2011). This unsupervised method groups days with similar diurnal shapes by minimizing within-cluster variance based on Euclidean distance. This well-known clustering technique has been applied in several previous studies related to the classification of solar daily profiles. The number of clusters was set to four, based on the analysis of the within-cluster variance and the physical interpretability of the resulting patterns. Each clusters centroid corresponds to a distinct intraday profile.

From a statistical standpoint, the silhouette score was used to determine the number of clusters (Rousseeuw, 1987). This metric quantifies on average how similar each element is to its assigned cluster compared with other clusters, providing a measure of cohesion (within-cluster compactness) and separation (between-cluster distinctness). Higher values indicate more effective partitioning of the data.

Finally, the frequency of occurrence of each cluster was evaluated separately for El Niño, La Niña, and neutral years. This allowed a quantitative assessment of how the prevalence of different types of solar days is modulated by ENSO conditions, complementing the results obtained from the analysis of daily aggregated GHI.

4. Results

4.1 Impact of the signal in daily irradiation

Figure 2 presents the mean hourly profiles of GHI for November-December, averaged separately according to El Niño, La Niña and neutral years. The results show a clear modulation of the irradiance according to different ENSO conditions. On average, Niño years (red) exhibit lower irradiance throughout the day, particularly near solar noon. Conversely, la Niña years (blue) tend to present higher irradiance levels. These results are consistent with previous results based on monthly accumulated irradiance (Laguarda et al., 2020a), which reported enhanced cloudiness and reduced solar irradiation during El Niño events. However, the present analysis extends those results by revealing that, during El Niño years, the reduction in irradiance occurs systematically at all hours of the day.

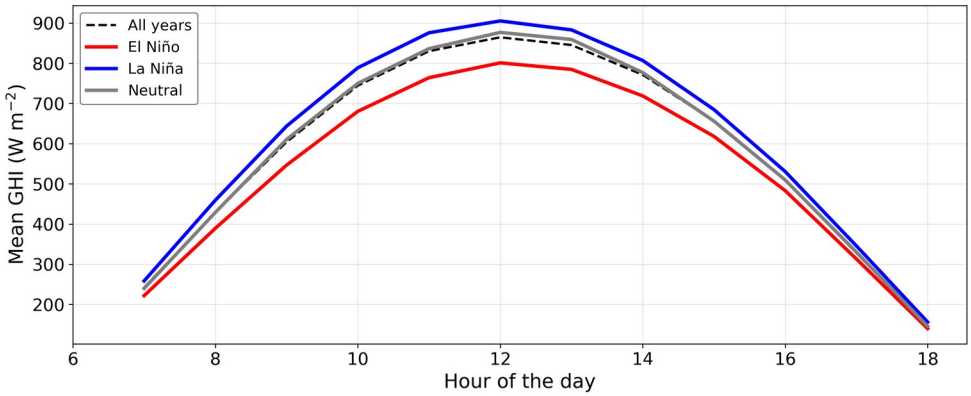

Figure 2. Mean hourly GHI profiles during November–December for El Niño (red), La Niña (blue), and neutral (grey) years. The dashed black line indicates the climatological mean (all years).

Figure 3 shows the cumulative distribution function (CDF) of daily kt during the ND period. The curve corresponding to El Niño years (red line) indicates a higher frequency of low daily kt values, consistent with the monthly-scale results reported in Laguarda (2020a). The absolute difference between the CDF of each ENSO phase and the overall distribution is shown in dashed lines (DIF. eq. 2). According to the K-S test, a DIF greater than 0.0134 indicates statistically significant differences between distributions (at p-value = 0.01). This condition is met for both El Niño and La Niña years, confirming that ENSO phases significantly

modulate the distribution of daily irradiance.

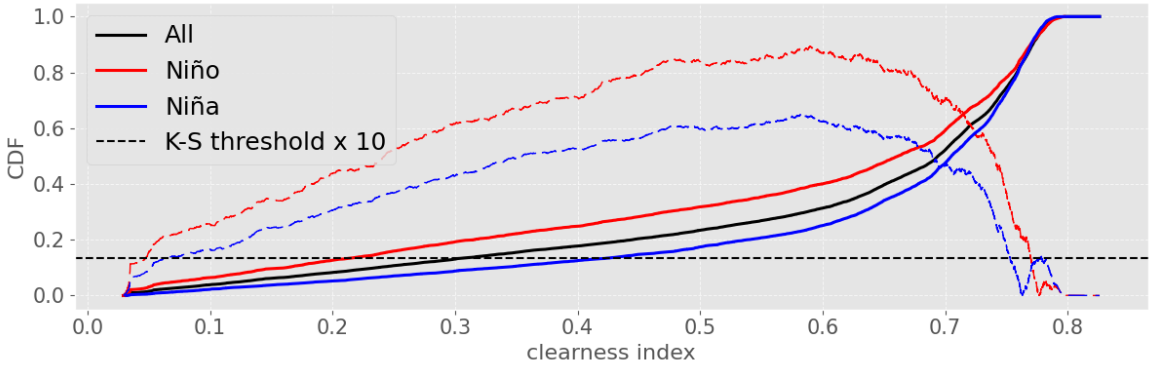

Figure 3. CDF of daily clearness index (kt) during November–December by ENSO phase. Dashed lines show the absolute difference with the ALL curve (scaled ×10). The threshold 0.0134 indicates significant difference at 1% level.

4.2 Clusterization of daily profiles and Impact of the ENSO signal

The daily profiles of kt were analyzed through a clustering approach using K-Means and euclidean distance. From a statistical standpoint, the silhouette score was used to evaluate the clustering performance varying the number of clusters (k) used. As shown in Figure 4, the silhouette score decreases for larger k values, indicating that additional clusters lead to poorer internal cohesion and weaker separation. Therefore, $k = 4$ was selected as the optimal compromise between statistical performance and physical interpretability.

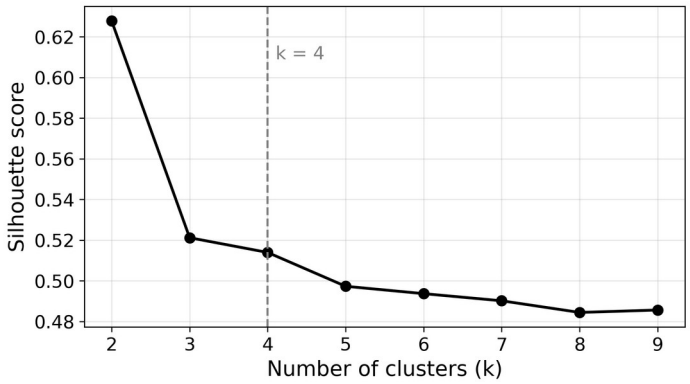

Figure 4. Silhouette score as a function of the number of clusters (k). The vertical dashed line indicates the selected value (k = 4), chosen as a trade-off between clustering performance and physical interpretability.

The procedure identified four distinct daily profiles (Figure 5):

1) Overcast days (named OC)

2) Clear days (named CL)

3) Days with clear mornings and cloudy afternoons (named CL-AM)

4) Days with cloudy mornings and clear afternoons (named CL-PM).

Overall, 65% of the 1418 profiles are identified as CL, while approximately 11% of the data falls in each remaining category. Similar results were obtained when clustering was based on GHI instead of kt, and for other northern Uruguay PV sites (not shown). Table 1 presents the percentage of days in each cluster,

separated by ENSO phase. Compared to the climatological mean (last column), OC days (Cluster 1) become more frequent during El Niño years (15.3%) compared to the climatological average (11.8%). Conversely, the frequency of CL days (Cluster 2) increases notably during La Niña events, rising from 65.0% to 72.7%, while it decreases markedly to 54.3% during El Niño events. Interestingly, the occurrence of CL-AM (Cluster 3) exhibits a clear modulation: it increases during El Niño (from 12.4 to 20.0%) and decreases during La Niña (to 7.7%). In contrast, the frequency of CL-PM (Cluster 4) remains relatively stable across ENSO phases.

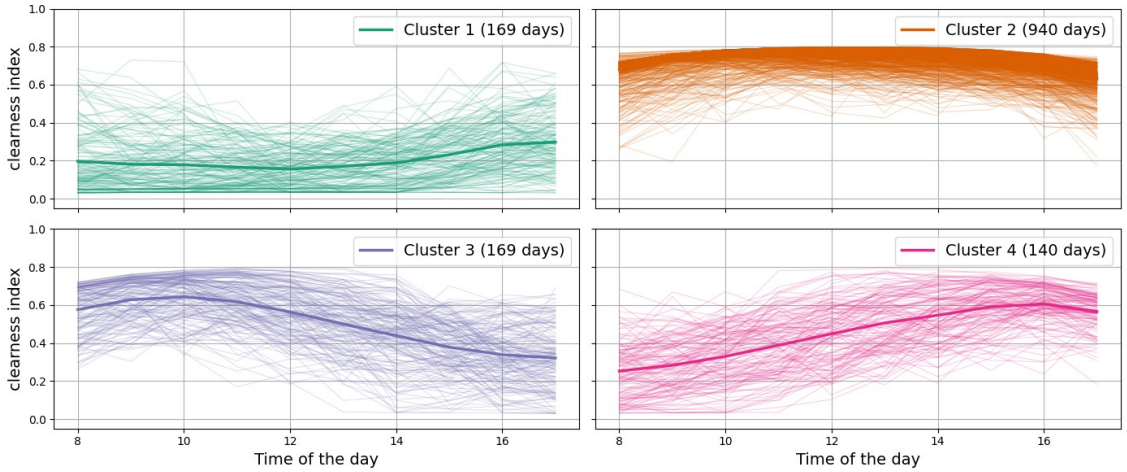

Figure 5. Daily kt profiles grouped into four clusters: Cluster 1 (OC), Cluster 2 (CL), Cluster 3 (CL-AM), Cluster 4 (CL-PM). Thin lines represent individual days, while the thicker line shows the mean profile of each cluster.

The last row in Table 1 reports the p-value from the Chi-square test, confirming that the cluster distributions under La Niña and El Niño conditions differ significantly. The Chi-square test was applied to the cluster frequencies across ENSO phases, testing the null hypothesis that the occurrence of each cluster is independent of ENSO conditions.

Table 1. Percentage of days in each cluster per ENSO phase and total. The last row reports the p-value from the Chi-square test, indicating that the cluster distributions during La Niña and El Niño years are statistically different.

	Neutral	La Niña	El Niño	All
Cluster 1 (OC)	13.0	8.8	**15.3**	11.8
Cluster 2 (CL)	65.0	**72.7**	54.3	65.0
Cluster 3 (CL-AM)	10.7	7.7	**20.0**	12.4
Cluster 4 (CL-PM)	11.3	10.8	10.4	10.8
p-value (Chi-Square vs All)	0.81019	**0.00081**	**0.00012**	NA

5. Conclusions

This study provides evidence that intraday solar irradiance profiles in northern Uruguay are significantly modulated by ENSO phases during November-December, the period most affected by ENSO. The clustering analysis revealed four distinct daily patterns of GHI (and kt), whose occurrence frequencies vary systematically with ENSO conditions in comparison with the climatology. La Niña years are associated with a higher prevalence of clear-sky days, while El Niño years show more overcast days and a marked increase

in days with clear mornings and cloudy afternoons. This last behavior is observed for the first time in relation to El Niño events. Although this analysis focuses on one representative site, similar behavior was found across the northern region, as supported by preliminary results. Ongoing work aims to extend the analysis to wider periods, particularly over February-May, which has also been identified as a relevant period for ENSO impacts. A detailed spatial distribution analysis of the results across the region is planned, along with a more comprehensive statistical assessment now possible with the full 24-year GHI series. Finally, efforts will be directed towards exploring the underlying physical mechanisms driving these patterns.

6. Acknowledgments

The authors would like to express their gratitude to the Universidad de la República (Udelar) for its continued support. A.L. and B.E. acknowledge the Comisión Sectorial de Investigación Científica (CSIC) for its support through the *CSIC Grupos* program. A.L. also acknowledges the Programa *Despegue Científico* of PEDECIBA for additional support.

7. References

Alonso-Suárez, R., Abal, G., Musé, P., y Siri, R. (2014). Satellite-derived solar irradiation map for Uruguay. In Elsevier Energy Procedia, 57:1237-1246.

De Vera, A. and Terra, R. (2018). A stochastic precipitation generator conditioned by a climate index. Journal of Applied Meteorology and Climatology, v.: 57 p.:2585 - 2603, 2018. DOI: https://doi.org/10.1175/JAMC-D-17-0307.1

Grimm, A., Barras, V. , and Doyle, M. (2000). Climate variability in southern South America associated with El Niño and La Niña events. J. of Climate, 13:35–58.

Laguarda, A., Alonso-Suárez, R., Abal, A. (2023). Improved estimation of hourly direct normal solar irradiation (DNI) using geostationary satellite visible channel images over moderate albedo areas. Solar Energy, 259:30-40.

Laguarda, Al, Iturbide, P, Orsi, X., Denegri, M.J., Luza, S., Burgos, L., Stern, V., Alonso-Suárez, R. (2021). Validación de los modelos satelitales Heliosat-4 y CIM-ESRA para la estimación de irradiancia solar en la Pampa Húmeda. Energías Renovables y Medio Ambiente, 48:1-9.

Laguarda, A., Alonso-Suárez, R., Terra, R., (2020a). Solar irradiation regionalization in Uruguay: Understanding the interannual variability and its relation to ENSO, Ren. Ener., 58,:444-452.

Laguarda, A., Giacosa, G., Alonso-Suárez, R., Abal, G., (2020b). Performance of the site-adapted CAMS database and locally adjusted cloud index models for estimating global solar horizontal irradiation over the Pampa Húmeda, Solar Energy, 199:295-307.

Massey, F. J. (1951). The Kolmogorov-Smirnov Test for Goodness of Fit. *Journal of the American Statistical Association*, *46*(253), 68–78. https://doi.org/10.1080/01621459.1951.10500769

McPhaden, M., Zebiak, S., Glantz, M. (2006). ENSO as an Integrating Concept in Earth Science. Science, 314: 1740.

Pisciottano, G., Díaz, A., Cazes, G., and C.R., M. (1994). El Niño-Southern Oscillation impact on rainfall in Uruguay. Journal of Climate, 7:1286 –1302.

Qu, Z., Oumbe, A., Blanc, P., Espinar, B., Gesell, G., Gschwind, B., Kl¨user, L., Lefevre, M., Saboret, L., Schroedter-Homscheidt, M., Wald, L. (2017). Fast radiative transfer parameterisation for assessing the surface solar irradiance: The Heliosat-4 method. Meteorologische Zeitschrift, 26(1):33–57.

Rigollier, C., Bauer, O., y Wald, L. (2000). On the clear sky model of the ESRA - European Solar Radiation Atlas - with respect to the Heliosat method. Solar Energy, 68(1):33–48.

Rousseeuw, P. (1987). Silhouettes: a Graphical Aid to the Interpretation and Validation of Cluster Analysis.

Computational and Applied Mathematics 20: 53-65.

Sengupta, M., Lopez, A., Habte, A., Maclaurin, G., Shelby, J. (2018). The National Solar Radiation Data Base (NSRDB). Renewable and Sustainable. Energy Reviews, 89, 51–60.

Trenberth, K. E. (1997). The definition of El Niño. Bulletin of the American Meteo. Soc., 78(12):2771–2778.

Wilks, D. S. (2011). *Statistical Methods in the Atmospheric Sciences* (3rd ed.). Academic Press.